Supporting Information:

Surface polarization enhances ionic transport and correlations in nanoconfined electrolyte solutions by conductors

Felipe Jiménez-Ángeles[a], Ali Ehlen[b], and Monica Olvera de la Cruz[a,b,c]
[a]Department of Materials Science and Engineering, Northwestern University, Evanston, Illinois 60208, USA
[b]Applied Physics Program, Northwestern University, Evanston, Illinois 60208, USA
[c]Department of Physics, Northwestern University, Evanston, Illinois 60208, USA

Molecular simulations for ion transport calculations

The simulations for calculating ion transport properties were run in LAMMPS version 23June2022 – Update 2[1]. All simulations of electrolyte solutions were run in a larger geometry, L_x = 10.1 nm and L_y = 10.2 nm, with a distance between electrodes of L_z = 0.97 nm. Accounting for excluded volume interactions between the carbon atoms of the electrodes and the water, the accessible space in the *z*-direction was $L_{z\text{-}effective}$ = ~0.63 nm. The number of water and ion molecules included in the simulations is below, with densities calculated using a slit volume of $L_x \times L_y \times L_{z-effective}$.

	NaCl	**$CaCl_2$**	**$LaCl_3$**
Number of water molecules N_w (water density)	2,264 (1.03 gm/cm^3)	2,192 (1.00 gm/cm^3)	2,264 (1.03 gm/cm^3)
Number of ions N_+, N_- (M cluster, M individual ions)	32, 32 (0.81 M, 1.6 M)	20, 40 (0.51 M, 1.5 M)	16, 48 (0.41 M, 1.6 M)

Table 1 Number of ions and water molecules in the transport properties simulations.

To simulate ion transport, the initial configurations for NaCl, $CaCl_2$, and $LaCl_3$ are generated using GROMACS[2, 3]. separately by equilibrating the electrolyte solution within the slit with a bulk electrolyte solution using the setup shown in Figure S1. The equilibrated slit region was isolated and replicated 2×2 times in the *x*- and *y*- directions. Then, the systems are simulated using LAMMPS with periodic boundary conditions in the *x*- and *y*-directions. For the $CaCl_2$ system, ions readily entered the slit, and the system was used as is. The NaCl and $LaCl_3$ systems required adjustment because ions did not easily enter the slit. For the NaCl system, we used the equilibrium concentration of NaCl ions in a separate GROMACS simulation of larger slit (L_z=12 Å) equilibrated with bulk electrolyte. We then replaced water molecules in the thinner slit case until they reached this concentration. For the $LaCl_3$ system, we used the initial configuration of the NaCl system, and changed the identity of ions to match the numbers in **Table *1***. We chose to keep the total number of ions roughly constant so that we could compare simulations with different salts without the additional complication of changing the number of ions, which could introduce other effects. We assume that the bulk salt concentrations required to achieve these conditions may be

much higher for NaCL and $LaCl_3$ than for $CaCl_2$—though why certain ions more easily enter the slit and under what conditions is another interesting question that we do not explore here.

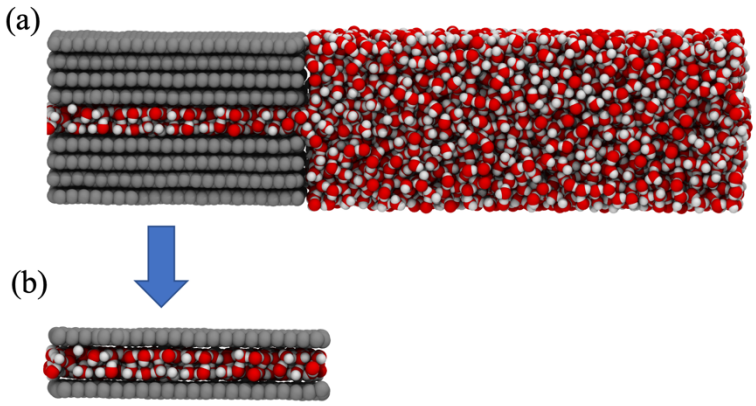

Figure S1: Equilibration between an aqueous solution confined within a slit-like pore and a bulk solution. (a) Simulation setup consisting of a slit pore region is formed by two surfaces in contact with a bulk aqueous solution. Each surface comprises four graphene layers of 5.05 nm × 5.1 nm. The simulation box dimensions are L_x = 14.03 nm, L_y = 5.1 nm, and L_z = 3.4 nm, in the x-, y-, and z-directions, respectively. The box contains 5484 water molecules. (b) After a simulation equilibration of 10 ns, the slit region is isolated, containing 580 water molecules, approximately. Then, the pore is replicated 2 × 2 times in the x- and y- directions. The equilibrated slit-like channel is transferred to LAMMPS to perform simulations at constant potential and constant charge.

Interactions between water, electrodes, and ions were modeling using the SPC/E water model and AA-OPLS force field[4, 5] parameters as described in the main text, and charged interactions are calculated using particle-particle-particle mesh solver with a slab correction to account for the quasi-two-dimensional geometry. Additionally, for polarizable electrodes (constant ψ), the ELECTRODE package in LAMMPS[1, 6] was applied to the carbon atoms of the electrodes to calculate interface polarization charge based on a constant potential constraint. All simulations were run at constant volume for 30 ns at 298 K, and the analysis was performed using the last 28 ns of the trajectory.

Charge of electrodes

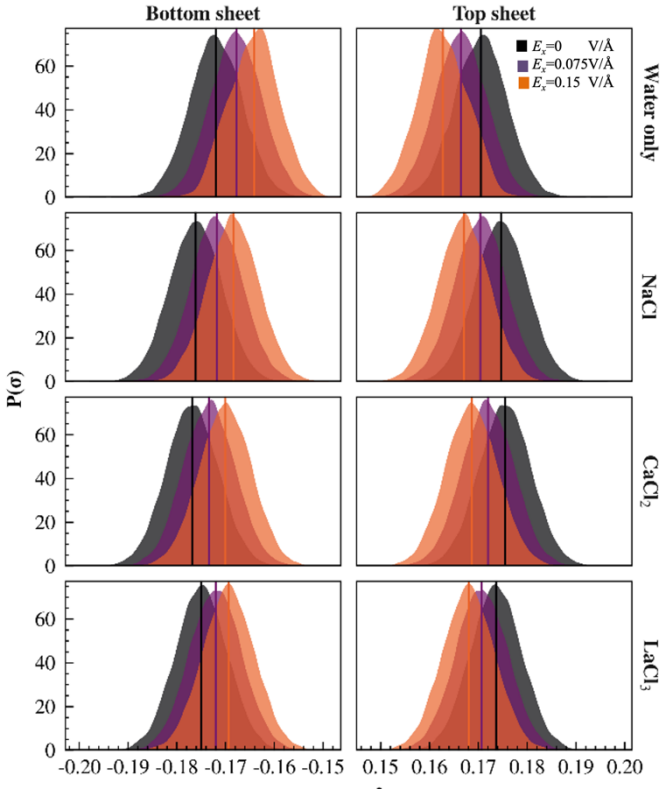

Figure S2: Histograms of charge densities on each electrode for simulations with polarizable electrodes an applied voltage of ψ = 0.5 V. The electric field (units of V/Å) applied parallel to the electrodes impacts the overall induced charge density, as does the ion type. The variance of σ is approximately the same in all simulations. At ψ=0, the induced charge density fluctuates around zero.

Ion density in the z direction colored by E-field

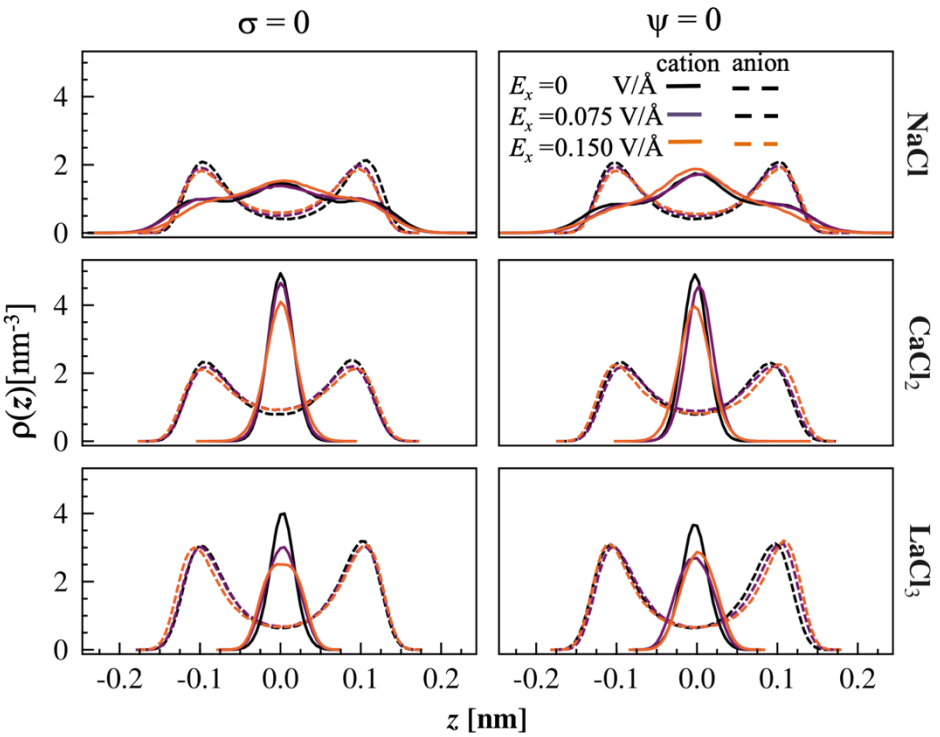

Figure S3: Ions number density profiles $\rho(z)$ as a function of the *z*-coordinate in gated channels. The solid lines represent the cations' profiles, whereas the dashed lines the anions' profiles. Anions tend to be adsorbed at the electrodes whereas cations remain in the channel's center, regardless of the valence. The effect of increasing electric field strength (units of V/Å) for higher-valency cations is to broaden their distribution. Ion density profiles and their response to external electric fields are similar for systems of conductors and non-polarizable materials.

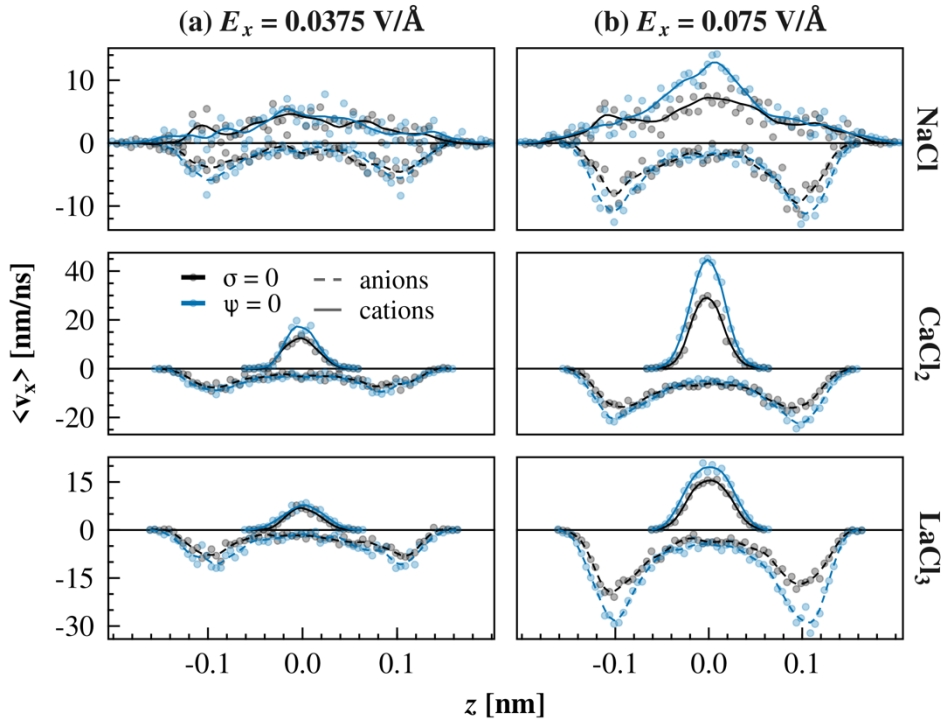

Figure S4 Average ions' velocity profiles in the *x*-direction $\langle \boldsymbol{v_x}(z) \rangle$ as a function of the coordinate *z*. The profiles are analogous to a local current of the ions with a dimensionless charge equal to 1. The velocity profiles are qualitatively similar to the density profiles (see Figure S3) but the anions' velocity is negative. Therefore, most of cations' transport occurs at the center of the slit whereas the anions' transport happens close to the surfaces. The comparison between slits made of non-polarizable surfaces and conductors shows that there are appreciable differences between the two systems even at moderately high fields. The points represent averages from the simulation data, and the lines are generated using a cubic spline to guide the eye. Averages are calculated as $\langle v_x(z) \rangle = \frac{1}{N_{\mathrm{fr}}} = \sum_{i=1}^{N_{\mathrm{fr}}} v_{x,i}(z)$ where $v_{x,i}(z)$ is the sum of the velocities of the particles within $(z, z + \delta z)$ at the *i*-th frame, and $\boldsymbol{N_{\mathrm{fr}}}$ is the number of frames in the simulation.

Ionic pair correlation functions in ungated slit-like channels of conductors and non-polarizable surfaces at different E-fields in the surfaces' parallel direction

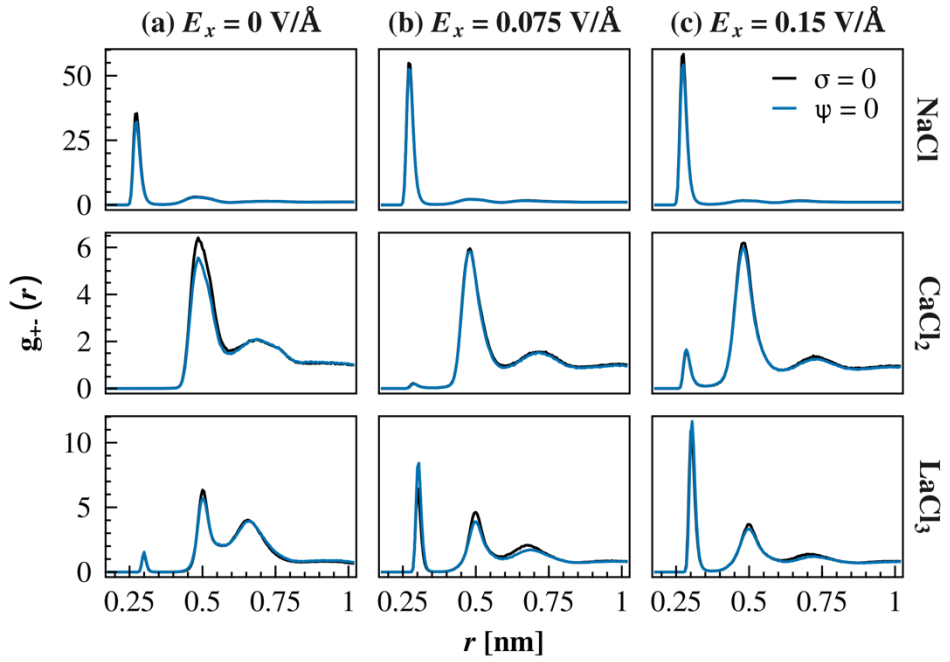

Figure S5: Cation-anion pair correlation functions $g_{+-}(r)$ of (a) NaCl, (b) $CaCl_2$, and (c) $LaCl_3$ confined by slit channels made of non-polarizable ($\sigma = 0$) and polarizable surfaces ($\psi = 0$). Each row contains the profiles at external fields of E_x = 0, 0.075, and 0.15 V/Å. Black lines represent the profiles in slit-like channels of conductors, while light-blue lines are in non-polarizable surfaces. The increasing peak just above 0.25 nm indicates increased ion pairing at higher applied fields.

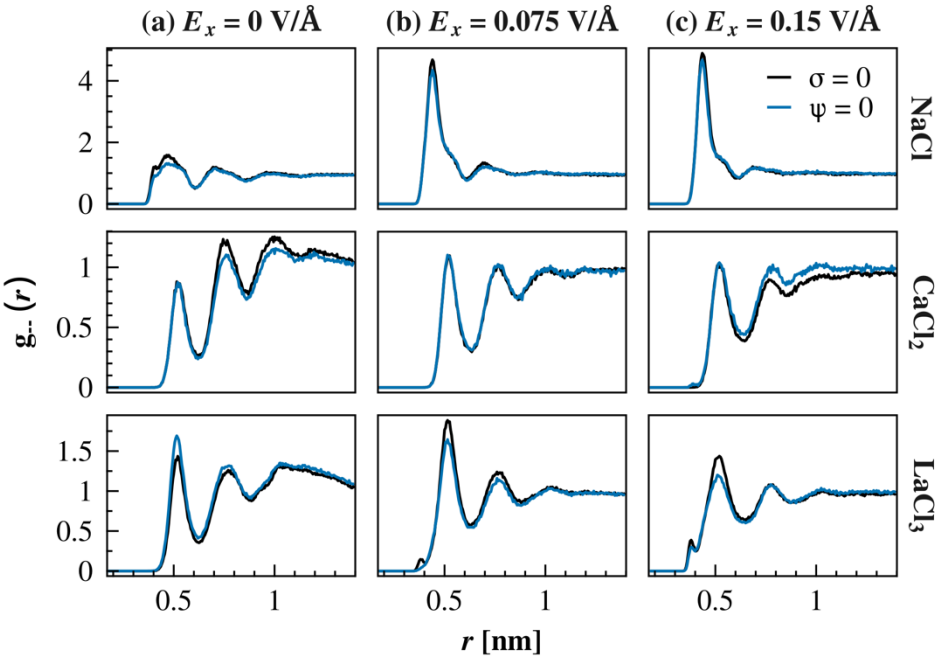

Figure S6: Anion-anion pair correlation functions $g_{--}(r)$ in (a) NaCl, (b) $CaCl_2$, and (c) $LaCl_3$ confined by slit channels made of non-polarizable ($\sigma = 0$) and polarizable surfaces ($\psi = 0$). Each row contains the profiles at external fields of E_x = 0, 0.075, and 0.15 V/Å. Black lines represent the profiles in slit-like channels of conductors, while light-blue lines are in non-polarizable surfaces.

Ion transport and density profiles in gated channels

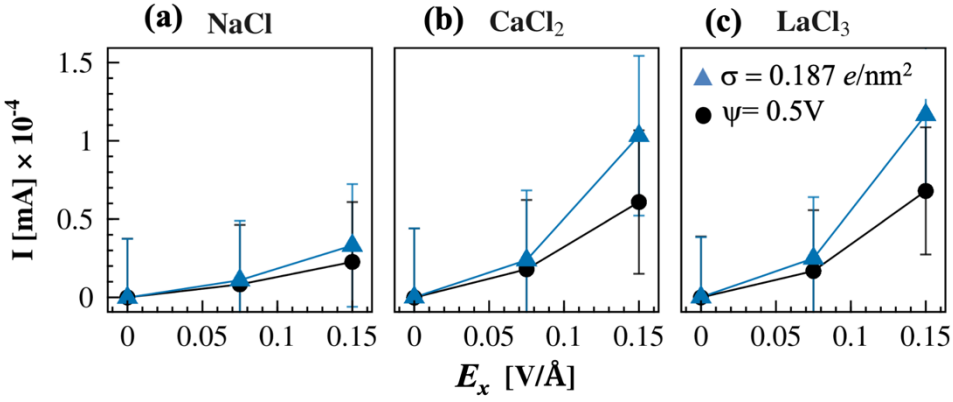

Figure S7: Ionic current in gated nanochannels. Average current as a function of the applied external field E_x of (a) NaCl, (b) $CaCl_2$, and (c) $LaCl_3$ electrolytes. The electrolytes are confined between charged non-polarizable surfaces (σ = 0.187 e/nm^2) and conductors ($\psi = 0.5$ V, $\Delta\psi = 1$ V). The separation distance between the surfaces is h = 0.97 nm.

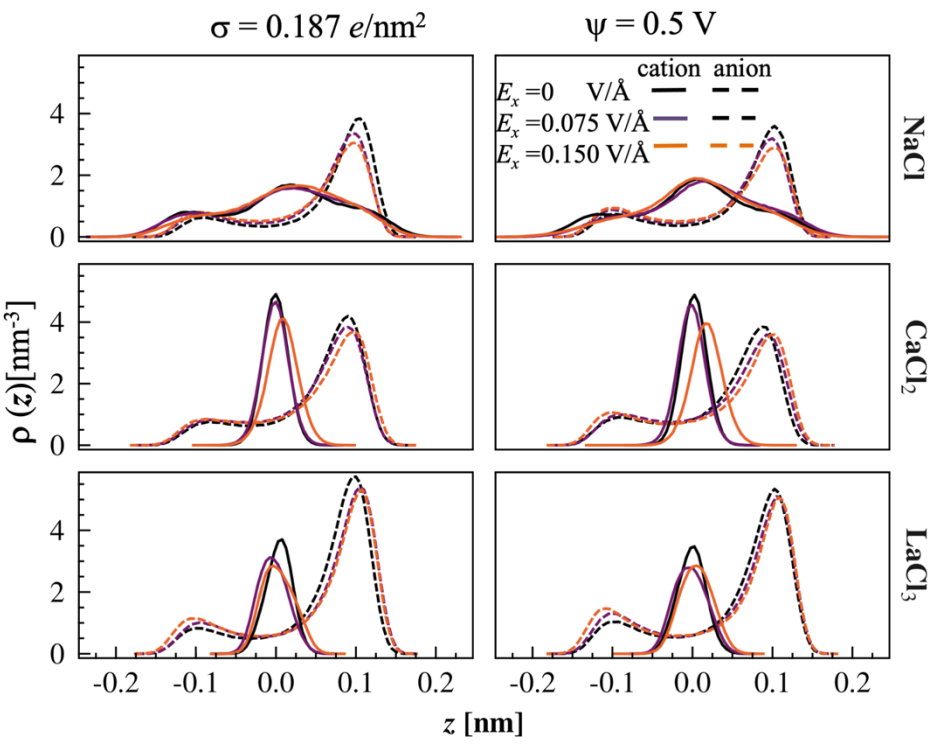

Figure S8: Ions number density profiles $\rho(z)$ as a function of the *z*-coordinate in gated channels. The solid lines represent the cations' profiles, whereas the dashed lines the anions' profiles. Anions tend to be adsorbed at the electrodes, whereas cations, regardless of species, tend to remain in the center of the slit. The effect of increasing electric field strength (units of V/Å) for higher-valency cations is to broaden their distribution. Ion density profiles and their response to external electric fields are similar for systems of conductors and non-polarizable materials.

Calculation of the Force between two oppositely charged ions at the middle plane between two parallel conductors using the image charge method

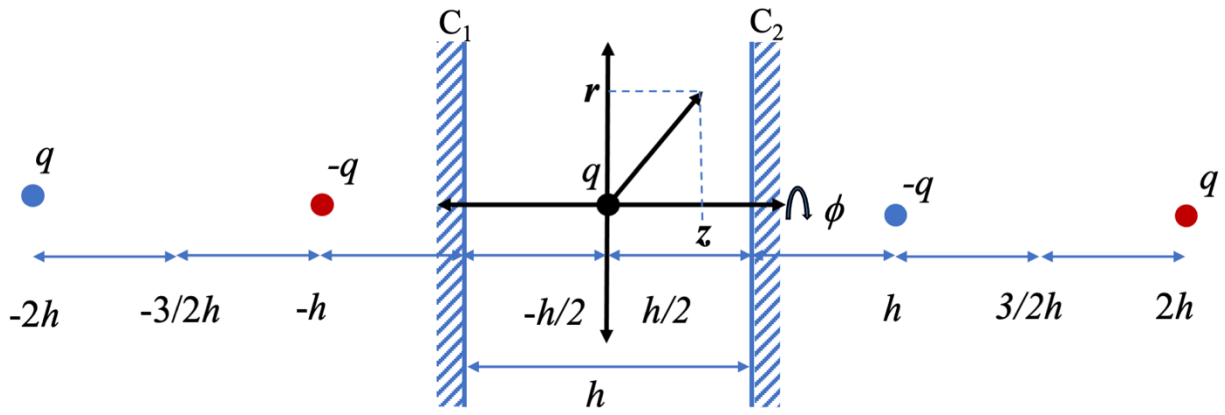

Figure S9: Schematic representation of two parallel conductors C_1 and C_2, with perpendicular separation distance *h*. A point charge *q* is placed at the middle plane between the two conductors and generates an infinite number of image charges at z = $\pm h/2$, $\pm h$, $\pm 3h/2$, $\pm 2h$… of the same magnitude and with an alternating sign. The positions are designated using a cylindrical coordinate system (r,ϕ,z) placed at the middle plane of the two surfaces.

Consider the system illustrated in Figure S8 consisting of two planar conductors parallelly placed with a separation distance *h*. A charge *q* is placed at the middle plane between the two conductors. The origin of a cylindrical coordinate system is placed at the location of the charge. We model the polarization charge using the image charge method. Due to the interaction of the charge with the conductors and between the conductors, an infinite number of image charges are induced in the system. The electrostatic potential at the position (*r*,*z*), considering the multiple image charges induced by the *q*, is expressed ad

$$\psi(z,r) = \frac{1}{4\pi\varepsilon_0}\frac{q}{(r^2+z^2)^{\frac{1}{2}}} - \frac{1}{4\pi\varepsilon_0}\left[\frac{q}{(r^2+(h-z)^2)^{\frac{1}{2}}} - \frac{q}{(r^2+(2h+z)^2)^{\frac{1}{2}}} + \frac{q}{(r^2+(3h-z)^2)^{\frac{1}{2}}} - \cdots\right]$$

$$- \frac{1}{4\pi\varepsilon_0}\left[\frac{q}{(r^2+(h+z)^2)^{\frac{1}{2}}} - \frac{q}{(r^2+(2h-z)^2)^{\frac{1}{2}}} + \frac{q}{(r^2+(3h+z)^2)^{\frac{1}{2}}} - \cdots\right]$$

(S 1)

In a more compact form, the electrostatic potential is written as

$$\psi(z,r) = \frac{1}{4\pi\varepsilon_0}\frac{q}{(r^2+z^2)^{\frac{1}{2}}} + \frac{1}{4\pi\varepsilon_0}\left[\sum_{n=1}^{\infty}\frac{(-1)^n q}{(r^2+(nh-z)^2)^{\frac{1}{2}}} + \sum_{n=1}^{\infty}\frac{(-1)^n q}{(r^2+(nh+z)^2)^{\frac{1}{2}}}\right]$$

(S 2)

We take the derivative of the potential with respect to the coordinate *z* to calculate the electric field in the *z*-direction, which gives

$$-E_z(r,z) = \frac{\partial\psi(z,r)}{\partial z} = \frac{-1}{4\pi\varepsilon_0}\frac{qz}{(r^2+z^2)^{\frac{3}{2}}} + \frac{1}{4\pi\varepsilon_0}\left[\sum_{n=1}^{\infty}\frac{(-1)^n q(nh-z)}{(r^2+(nh-z)^2)^{\frac{3}{2}}} + \sum_{n=1}^{\infty}\frac{(-1)^{n+1} q(nh+z)}{(r^2+(nh+z)^2)^{\frac{3}{2}}}\right]$$

(S 3)

The polarization charge density on the conductor is given as

$$\sigma_p = \varepsilon_0 \left.\frac{\partial\psi(z,r)}{\partial z}\right|_{z=\frac{h}{2}}$$

$$= \frac{-1}{4\pi}\frac{qh}{\left(r^2+(\frac{h}{2})^2\right)^{\frac{3}{2}}} + \frac{1}{4\pi}\left[\sum_{n=1}^{\infty}\frac{(-1)^n q(nh-h/2)}{(r^2+(nh-h/2)^2)^{\frac{3}{2}}} + \sum_{n=1}^{\infty}\frac{(-1)^{n+1} q(nh+h/2)}{(r^2+(nh+h/2)^2)^{\frac{3}{2}}}\right]$$

(S 4)

The total polarization charge q_p on one of the conductors is

$$q_p = \int \sigma_p dA = \int_0^{\infty} \sigma_p 2\pi r dr = -\frac{q}{2}$$

(S 5)

Which is exactly one half of the charge because the polarization charge is distributed symmetrically in the two conductors.

The electric field in the surfaces' parallel direction is given as

$$E_r = -\frac{\partial\psi(z,r)}{\partial r} = \frac{1}{4\pi\varepsilon_0}\frac{qr}{(r^2+z^2)^{\frac{3}{2}}} - \frac{1}{4\pi\varepsilon_0}\left[\sum_{n=1}^{\infty}\frac{(-1)^{n+1} qr}{(r^2+(nh-z)^2)^{\frac{3}{2}}} + \sum_{n=1}^{\infty}\frac{(-1)^{n+1} qr}{(r^2+(nh+z)^2)^{\frac{3}{2}}}\right]$$

(S 6)

The force on a charge q' located at the middle plane of the two conductors is given as

$$F_r(z=0,r) = q' E_r(z=0,r) = \frac{1}{4\pi\varepsilon_0}\frac{q'q}{r^2} - \frac{q'q}{2\pi\varepsilon_0}\left[\sum_{n=1}^{\infty}\frac{(-1)^{n+1} r}{(r^2+(2nh)^2)^{\frac{3}{2}}}\right]$$

(S 7)

References

1. Thompson, A. P.; Aktulga, H. M.; Berger, R.; Bolintineanu, D. S.; Brown, W. M.; Crozier, P. S.; in 't Veld, P. J.; Kohlmeyer, A.; Moore, S. G.; Nguyen, T. D.; Shan, R.; Stevens, M. J.; Tranchida, J.; Trott, C.; Plimpton, S. J., LAMMPS - a flexible simulation tool for particle-based materials modeling at the atomic, meso, and continuum scales. *Computer Physics Communications* **2022,** *271*, 108171.
2. Hess, B.; Kutzner, C.; van der Spoel, D.; Lindahl, E., GROMACS 4: Algorithms for Highly Efficient, Load-Balanced, and Scalable Molecular Simulation. *Journal of Chemical Theory and Computation* **2008,** *4* (3), 435-447.
3. Páll, S.; Zhmurov, A.; Bauer, P.; Abraham, M.; Lundborg, M.; Gray, A.; Hess, B.; Lindahl, E., Heterogeneous parallelization and acceleration of molecular dynamics simulations in GROMACS. *The Journal of Chemical Physics* **2020,** *153* (13), 134110.
4. Jorgensen, W. L.; Maxwell, D. S.; Tirado-Rives, J., Development and Testing of the OPLS All-Atom Force Field on Conformational Energetics and Properties of Organic Liquids. *Journal of the American Chemical Society* **1996,** *118* (45), 11225-11236.
5. Berendsen, H. J. C.; Grigera, J. R.; Straatsma, T. P., The missing term in effective pair potentials. *The Journal of Physical Chemistry* **1987,** *91* (24), 6269-6271.
6. Ahrens-Iwers, L. J. V.; Meißner, R. H., Constant potential simulations on a mesh. *The Journal of Chemical Physics* **2021,** *155* (10), 104104.